Chemistry Europe
European Chemical Societies Publishing

WILEY VCH

Excellence in Chemistry Research

Announcing our new flagship journal

- Gold Open Access
- Publishing charges waived
- Preprints welcome
- Edited by active scientists

Meet the Editors of *ChemistryEurope*

Luisa De Cola
Università degli Studi di Milano Statale, Italy

Ive Hermans
University of Wisconsin-Madison, USA

Ken Tanaka
Tokyo Institute of Technology, Japan

Chemistry–A European Journal

Research Article
doi.org/10.1002/chem.202203443

Chemistry Europe
European Chemical Societies Publishing

www.chemeurj.org

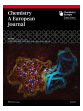

Specific Signal Enhancement on an RNA-Protein Interface by Dynamic Nuclear Polarization

Victoria Aladin[+],[a, b] Arun K. Sreemantula[+],[c] Thomas Biedenbänder,[a, b] Alexander Marchanka,*[c, d] and Björn Corzilius*[a, b, e]

Abstract: Sensitivity and specificity are both crucial for the efficient solid-state NMR structure determination of large biomolecules. We present an approach that features both advantages by site-specific enhancement of NMR spectroscopic signals from the protein-RNA binding site within a ribonucleoprotein (RNP) by dynamic nuclear polarization (DNP). This approach uses modern biochemical techniques for sparse isotope labeling and exploits the molecular dynamics of ^{13}C-labeled methyl groups exclusively present in the protein. These dynamics drive heteronuclear cross relaxation and thus allow specific hyperpolarization transfer across the biomolecular complex's interface. For the example of the L7Ae protein in complex with a 26mer guide RNA minimal construct from the box C/D complex in archaea, we demonstrate that a single methyl-nucleotide contact is responsible for most of the polarization transfer to the RNA, and that this specific transfer can be used to boost both NMR spectral sensitivity and specificity by DNP.

Introduction

Knowledge of the three-dimensional structure of a biomolecule is crucial for understanding its function and role, for example, in the context of a cellular process, and is also equally important in the development and design of new drugs.[1] NMR spectroscopy is a valuable method for structure determination with atomic resolution. Especially in cases where long-range order is absent, NMR often is the method of choice. Particularly for large or insoluble biomolecular systems, solid-state NMR (ssNMR) in combination with magic-angle spinning (MAS) can provide sufficient spectral resolution and is, in principle, not limited by molecular size.[2] However, particularly for large biomolecular systems, the applicability of ssNMR may become practically limited by spectral crowding and/or sensitivity. The latter is exacerbated by the fact that NMR is an inherently insensitive method; thus, the limited sample amount might lead to prohibitively long signal acquisition times on the order of at least weeks to months for multi-dimensional nuclear correlation experiments.[3] In this case, dynamic nuclear polarization (DNP) can significantly increase the sensitivity of NMR by transferring the large thermal polarization of unpaired electrons to nuclear spins under microwave irradiation.[4] Here, enhancements in the NMR sensitivity for a biomolecular system up to the factor of ~250 have been demonstrated.[5] Factors of 10 to 100 are generally obtained even at the largest magnetic fields, resulting in time savings of at least two orders of magnitude.

Spectral crowding arises from the fact that the incredible variety of biomolecules is remarkably based on just a few chemically similar building blocks such as nucleotides, amino acids and carbohydrates. This poses a significant challenge for spectral resolution and resonance assignment. Also, specific isotope-labeling of selected residues is difficult if the biomolecules are produced by biochemical methods such as recombinant expression or transcription. As a result, structural NMR studies of biomolecules or biomolecular complexes of increasing size are presenting a steep complexity problem; this problem is even exacerbated in the case of nucleic acids where only four different nucleotides with rather small chemical shift dispersion make up biopolymers of at least tens to hundreds of monomers. Therefore, even with the immense sensitivity enhancement by DNP, the examination of large biomolecular

[a] Dr. V. Aladin,[+] T. Biedenbänder, Prof. Dr. B. Corzilius
Institute of Chemistry
University of Rostock
Albert-Einstein-Str. 27, 18059 Rostock (Germany)
E-mail: bjoern.corzilius@uni-rostock.de
Homepage: http://www.corzilius.chemie.uni-rostock.de

[b] Dr. V. Aladin,[+] T. Biedenbänder, Prof. Dr. B. Corzilius
Department Life, Light & Matter, University of Rostock
Albert-Einstein-Str. 25, 18059 Rostock (Germany)

[c] A. K. Sreemantula,[+] Dr. A. Marchanka
Institute for Organic Chemistry and
Centre of Biomolecular Drug Research (BMWZ)
Leibniz University Hannover
Schneiderberg 38, 30167, Hannover (Germany)
E-mail: alexander.marchanka@oci.uni-hannover.de

[d] Dr. A. Marchanka
Structural and Computational Biology Unit
European Molecular Biology Laboratory
Meyerhofstr. 1, 69117 Heidelberg (Germany)

[e] Prof. Dr. B. Corzilius
Leibniz Institute for Catalysis
Albert-Einstein-Str. 29, 18059 Rostock (Germany)

[+] These authors contributed equally to this work.

Supporting information for this article is available on the WWW under https://doi.org/10.1002/chem.202203443

systems remains challenging due to the additional necessity of resolution or specificity.

In order to increase spectral specificity, several techniques exist and are often applied in combination. Among those are selective isotope labeling protocols, dedicated NMR methods, as well as utilization of temperature-activated dynamics. While the first two points can be more or less controlled by the choice of sample preparation route or selection of appropriate pulse sequence, the latter is an inherent biomolecular property and may only be affected indirectly by means of experimental conditions, in particular temperature and, to a lesser degree, external magnetic field strength.

The threefold reorientation dynamics of methyl groups have been extensively exploited in high-resolution NMR. In recent decades the further development of transverse relaxation-optimized spectroscopy (TROSY)[6] to methyl groups by the Kay group[7] allowed to extend the access to structural and motional information for protein complexes as large as 1 MDa.[8] Methyl-TROSY relies on selective ^{1}H,^{13}C labeling of methyl groups in fully deuterated proteins and utilizes the fact that the motions of methyl groups are strongly decoupled from the slow overall molecular tumbling;[9] as a result, they exhibit slow transverse relaxation and thus narrow spectral lines in heteronuclear multiquantum correlation (HMQC) spectra.[7a] As methyl groups in protein side chains are distributed uniformly across the protein they can be used to probe intra- and intermolecular distances in multi-component protein assemblies and provide information about dynamics.

In solution, dynamics may also be probed or used by nuclear Overhauser effect spectroscopy (NOESY);[10] where fluctuations of dipolar homo- or heteronuclear interactions result in cross-relaxation-based polarization transfer between coupled nuclei subject to molecular motion.[11] In the solid state, such effects are usually small due to largely arrested dynamics on the timescale of the inverse nuclear Larmor frequency. Nevertheless, several cases of heteronuclear Overhauser effect (hetNOE) have been reported in crystalline solids[12] and proteins,[13] polymers,[14] or within solid-liquid interfaces.[15] Particularly, the dynamics of methyl groups or homologs have been exploited by this effect,[16] which has also been demonstrated as an alternative to $^{1}H-^{13}C$ cross polarization for uniform signal enhancement of ^{13}C in fully labeled solids.[17]

One limitation of hetNOE lies in the limited polarization that can be transferred between different nuclides. Derived from the Solomon equations describing the relaxation of two coupled spins,[11] the hetNOE Equation (1) quantifies the attainable relative polarization on the observed nucleus:

$$\varepsilon_{\mathrm{hetNOE}} = 1 + s\frac{\gamma_{\mathrm{H}}}{\gamma_{\mathrm{C}}}\frac{\sigma_{\mathrm{HC}}}{\rho_{\mathrm{C}}} \tag{1}$$

Here, s is the ^{1}H saturation factor, γ_{H} and γ_{C} denote the gyromagnetic ratios of ^{1}H and ^{13}C, respectively, whereas σ_{HC} and ρ_{C} represent the ^{1}H–^{13}C cross-relaxation and the ^{13}C auto relaxation rates, respectively. The saturation factor,

$$s = \frac{P_{\mathrm{H}}^{\circ} - P_{\mathrm{H}}}{P_{\mathrm{H}}^{\circ}}, \tag{2}$$

reaches $s=1$ at full saturation (i.e., the ^{1}H polarization is fully depleted with $P_{\mathrm{H}}=0$) by rf irradiation during the hetNOE buildup period. If ^{1}H polarization is at its thermal equilibrium value, P_{H}°, then $s=0$ and the hetNOE vanishes with $\varepsilon_{\mathrm{hetNOE}}=1$. The ratio between cross and auto relaxation (often denoted the coupling factor) cannot be larger than unity; thus, the relative polarization gain is thus limited to the ratio of the gyromagnetic factors between the irradiated and observed nucleus. This effectively limits the maximum hetNOE gain on ^{13}C to a factor of ~4.

In 2016 it has been shown that hyperpolarized ^{1}H can spontaneously induce a similar hetNOE-like transfer within dynamical functional groups during DNP.[18] Thus, this effect has been named specific cross relaxation enhancement by active motions under DNP (SCREAM-DNP).[19] In contrast to a typical hetNOE experiment, the polarization transferred to methyl-^{13}C is not originating from the saturated Zeeman polarization of ^{1}H, but is based on the strongly hyperpolarized ^{1}H reservoir due to DNP. Consequentially, Equation (2) may be rewritten in Equation (3) as

$$\frac{P_{\mathrm{H}}^{\circ} - P_{\mathrm{H}}}{P_{\mathrm{H}}^{\circ}} = 1 - \varepsilon_{\mathrm{DNP}}. \tag{3}$$

This increases the effective polarization transfer by the DNP enhancement factor,

$$\varepsilon_{\mathrm{SCREAM-DNP}} = 1 - (\varepsilon_{\mathrm{DNP}} - 1)\frac{\gamma_{\mathrm{H}}}{\gamma_{\mathrm{C}}}\frac{\sigma_{\mathrm{HC}}}{\rho_{\mathrm{C}}}, \tag{4}$$

such that a maximum gain of ~2600-fold is possible from Equation (4). Given that, experimentally, the DNP enhancement factor is typically on the order of 50–200, direct polarization enhancement of several-hundred-fold becomes achievable. Therefore, even weak/slow molecular dynamics at ~100 K with rather small coupling factors allow for a sizeable sensitivity gain.

As mentioned above, methyl groups feature significant mobility at low temperatures and are thus excellent promotors for cross-relaxation transfer which results in a highly specific accumulation of enhanced magnetization in the direct vicinity of a ^{13}C-labeled methyl group.[20] Besides the three-fold reorientation dynamics of methyl groups, this effect has also been shown to be emerging from polyethylene glycol chains,[21] five- and six-membered ring dynamics,[20–21] and $^{15}NH_3^+$ groups.[22] In contrast to site-specific or localized DNP by tagging the biomolecule of interest with a polarizing agent, this approach has the advantage that no strong paramagnetic interactions are observed in the sought-after spectra, and that the spreading of the nuclear polarization specifically transferred to ^{13}C can be much more restricted and better controlled as compared to the direct DNP transfer.[18a,23] This has recently allowed us to selectively detect nuclear spin coherences from

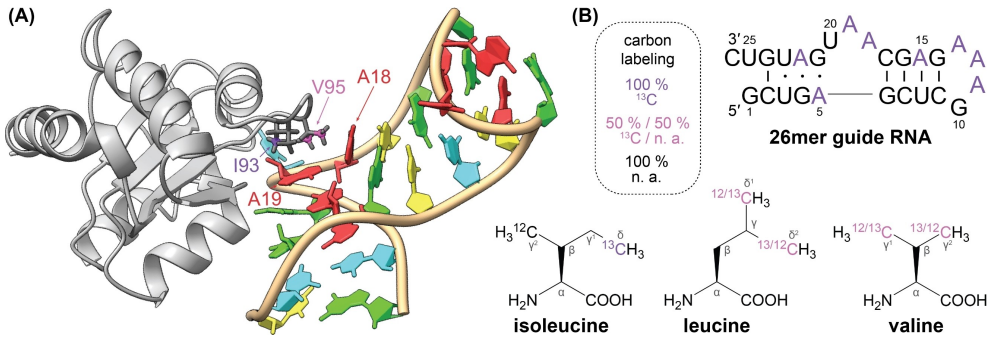

Figure 1. A) Depiction of the L7Ae-wt + RNA complex (ssNMR structure PDB ID: 6TPH).[29b] Color code: gray: L7Ae protein (residues I93 and V95 in dark gray, with their methyl carbons in purple and pink, respectively), light brown: RNA backbone, red: A, green: G, blue: C, yellow: U. B) Carbon isotope labeling scheme of Ile, Leu, and Val amino acids (purple carbons are fully ^{13}C labeled, pink are alternately labeled on one side-chain methyl each) as well as secondary structure of the 26mer guide RNA (adenosines in red are uniformly labeled). All other residues in L7Ae and RNA are in natural abundance of carbon isotopes.

bound biomolecular complexes in the presence of unbound constituents,[24] or to selectively probe the binding pocket of a retinal protein.[25]

Recognizing the high potential of SCREAM-DNP for the study of interaction surfaces, we have applied this approach to characterize protein-RNA interactions in the box C/D ribonucleoprotein (RNP). Box C/D RNP performs posttranscriptional 2′-O-ribose methylation of rRNA in archaea and eukaryotes.[26] The box C/D complex in archaea consists of three core proteins assembled around the guide small RNA and its structure has been obtained in great detail by a solution-state NMR-based integrative structural biology approach.[27] The 13.5 kDa L7Ae protein binds guide RNA and constitutes the crucial platform for further assembly of the 370 kDa large box C/D RNP.[28] A minimal box C/D RNA construct (26mer) in complex with L7Ae protein has been extensively studied by ssNMR spectroscopy and its structure has been reported recently;[29] a graphical representation is shown in Figure 1A. In this study we show the application of SCREAM-DNP to this crucial part of box C/D RNP assembly by utilizing the endogenous methyl groups of amino acids in L7Ae as SCREAM-DNP source. The absence of methyl groups in the (unmodified) RNA in combination with sparse ^{13}C-labeling of the protein (as shown in Figure 1B) makes this approach highly selective, resulting exclusively in NMR signals emanating from magnetization transferred from the protein to the RNA at the immediate interface where protein methyl groups are in direct dipolar contact with adenosines in the nucleic acid.

Results and Discussion

In order to investigate the temperature dependence of methyl dynamics and its impact on MAS NMR spectra and DNP enhancement we acquired DNP-enhanced ^{1}H,^{13}C CPMAS NMR spectra of $^{13}C_{10}$,$^{15}N_5$-adenosine-labeled 26mer box C/D RNA (with uridine, cytidine, and guanosine in natural isotope abundance; from hereon called ^{13}C,^{15}N A^{lab} RNA) in complex with the L7Ae wild type protein featuring ^{2}H-γ,δ2-[^{1}H,^{13}C-δ1 methyl]-Leu, ^{2}H-β,γ1-[^{1}H,^{13}C-γ2 methyl]-Val, ^{2}H-γ-[^{1}H,^{13}C-δ methyl]-Ile L7ae (from hereon called δ-$^{13}CH_3$ ILV-L7Ae-wt) at different temperatures. As shown in Figure 2, the effect of the unique dynamics of methyl groups are clearly visible with the three-fold reorientation being active even at typical DNP temperatures of 100 K due to their relatively small activation energies. At this temperature their dynamics can interfere with typical frequencies applied during solid state NMR experiments for recoupling, decoupling or MAS, leading to line broadening or even a full disappearance of the methyl signal.[30] This can be seen in the spectrum as a significant reduction in intensity of the methyl region (between 30 and 10 ppm) when decreasing the temperature. At the same time, the signal intensity of the rest of the spectrum strongly increases towards lower temperature due to the requirement of DNP enhancement on a slowly relaxing, rigid dipolar spin network. Therefore, by varying the temperature the signal loss from methyl dynamics can be avoided, however, a compromise must be found where the overall DNP enhancement is still satisfactory. In our investigated case, the absolute methyl MAS NMR signal was maximal at a temperature of 146 K, even though the overall DNP enhanced

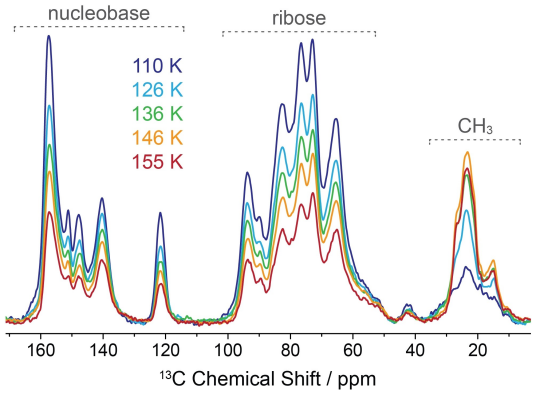

Figure 2. DNP-enhanced ^{1}H,^{13}C CPMAS spectra of ~0.4 mM δ-$^{13}CH_3$ ILV-L7Ae-wt + ^{13}C,^{15}N A^{lab} RNA complex in d_8-$^{12}C_3$-glycerol/D_2O/H_2O (50:40:10 vol.–%) with 15 mM AMUPol at 8 kHz MAS and 3 s of polarization time at different temperatures. Due to the specific ^{13}C labeling, the protein methyl (ILV) resonances and the resonances of adenine nucleobase as well as the riboses are clearly separated into the spectral regions as indicated.

signal intensity was reduced to ~50%. We have therefore chosen this temperature regime for all following experiments.

In order to identify dipolar contacts between protein methyls and RNA for potential polarization transfer we have recorded 2D DARR (dipolar-assisted rotational resonance) $^{13}C,^{13}C$ correlation spectra with longitudinal homonuclear mixing times up to 200 ms under DNP conditions (see the Supporting Information). For RNA in hydrogen natural abundance, only one strong and one weak contact between a methyl group and adenosine could be found (Figure S1A in the Supporting Information). The indirect dimension chemical shift of 12.7 ppm is in agreement with the previous assignment to I93δ.[29b] Furthermore, we tentatively assigned the contact at a direct dimension chemical shift of 156.7 ppm to C6 of A19 based on previous assignments and the ssNMR structure PDB ID: 6TPH where the distance to the I93δ methyl group and C6 is rather short with 4.5 Å (Table S1).[29b] The methyl assignment is further supported by a significant upfield shift of the I93δ resonance occurring below 13 ppm which may be caused by ring currents of the aromatic purine heterocycle; in the ssNMR structure, the methyl group is situated almost exactly above the aromatic plane which would lead to significant shielding of the ^{13}C nucleus. We also find a much weaker crosspeak at a direct chemical shift of 150.6 ppm, however, with a slight spurious deviation in the indirect dimension. Due to the perfect agreement with the expected shift for A19–C4 which should have the shortest distance to I93δ at only 3.9 Å we believe that this deviation is caused by the rather poor signal-to-noise ratio despite the significant DNP enhancement. It is not fully clear, why this contact together with the other expected contacts to I93δ with shorter distances (i.e., A19–C5 with 4.1 Å, or C8 with 4.3 Å) are so much weaker or not observed at all in comparison with the strong C6 resonance.

Interestingly, by full perdeuteration of the RNA (i.e., incorporating $^{2}H_{11},^{13}C_{10},^{15}N_5$-adenosine, $^{2}H_{10}$-uridine, $^{2}H_{11}$-cytidine, and $^{2}H_{11}$-guanosine; short $^{2}H,^{13}C,^{15}N$ A^{lab}, ^{2}H U,G,C^{lab} RNA) we have been able to dramatically increase the crosspeak intensity for methyl-adenosine contacts and reveal the above-mentioned missing contacts (Figure S1B). This is caused by a reduction of unspecific relayed transfer through the ^{13}C network within the RNA upon removal of spin-diffusion driving protons. Deuteration of the RNA revealed not only contacts between I93δ and A19 for all its nucleobase and ribose resonances, but also crosspeaks of a second methyl group at an indirect chemical shift of 20.9 ppm in contact with nucleotide resonances. Based on the chemical shift assignment and the solid-state NMR structure,[29b] we attribute this latter methyl's contacts to V95γ1–A18. Noticeably, in this case, we observe the contacts to almost all carbons of the adenine nucleobase (with the exception of C2) but none of adenosine's ribose. This is in agreement with the shorter distances between V95γ1 and A18's nucleobase carbons which are below 5 Å (with C4, C5, and C6 being significantly below 4 Å), whereas the ribose carbons are at least 5 Å away from the methyl carbon (with the exception of C2′ being at a distance of 4.7 Å). At 100 ms mixing, only one crosspeak from V95γ1 to A18–C5 remains due to the very short distance of only 3.6 Å (Figure S1C). Interestingly, the intensity of the V95γ1–A18 nucleobase crosspeaks is much weaker than those between I93δ and A19, even though the average distances between the former are generally shorter. Here, it should be reminded that with the ILV-labeling scheme used, V95γ1 is ^{13}C labeled with only 50% efficiency, while the alternately labeled V95γ2 points in the direction opposite to A18 without any methyl-adenosine distances below 5 Å. Therefore, we expect that the crosspeak intensities from V95 would also be reduced by 50% labeling efficiency.

In contrast to these DNP-enhanced experiments at low-temperature, by using conventional high-field MAS NMR at 275 K we have only been able to observe a single crosspeak between a methyl resonance and an adenosine (Figure 3). Somewhat surprisingly, this crosspeak is not one of the contacts observed at low temperature, as a significant upfield shift is observed both in the indirect dimension with respect to the V95γ1 resonance and in the direct dimension with respect to the A18–C2 resonance. However, the direct dimension chemical shift (154.5 ppm) is in perfect agreement with the earlier observed shift for A19–C2 (which has been recorded under similar conditions),[29a] while at low temperature this resonance is upfield shifted by 1.0 ppm. Therefore, we assign this resonance to the contact from V95γ2 to this nucleobase carbon

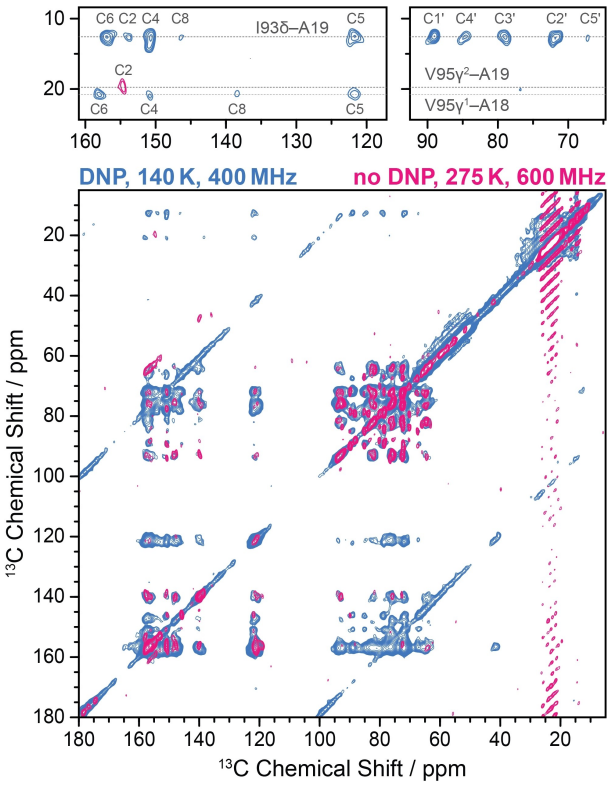

Figure 3. Comparison between $^{1}H,^{13}C$ CP-based 2D $^{13}C,^{13}C$ correlation spectra of the δ-$^{13}CH_3$ ILV-L7Ae-wt + $^{2}H,^{13}C,^{15}N$ A^{lab}, ^{2}H U,G,C^{lab} RNA complex. The magenta spectrum was recorded under conventional MAS NMR conditions at 600 MHz, 14 kHz MAS, 275 K, and 14 ms RFDR recoupling. The blue spectrum was recorded with DNP enhancement at 400 MHz, 8 kHz MAS, 140 K, and 200 ms DARR recoupling. The two subplots on top show magnifications of the regions where contacts between methyls and adenosine nucleobase (left) and ribose (right) atoms are found.

due to the very short proposed distance of only 3.5 Å as well as the good match of the methyl chemical shift (expected at 20.1 ppm).[29b] A discrepancy between the A19–C2 chemical shift at room and low temperature is not unexpected. The adenine C2 chemical shift is highly sensitive to its surroundings and the exocyclic torsion angle,[31] therefore, a small local change may be induced under cryogenic conditions. Besides this, the overall congruence of 2D resonances at room and low temperature is rather good, suggesting only very minor changes in the complex's structure upon freezing. In light of the V95γ2–A19–C2 peak being the only strong contact at room temperature, its absence at low temperature might seem surprising. However, the methyl dynamics of this V95γ2 group is most likely interfering with NMR detection particularly at low temperature; the strong dependence of methyl resonance intensities on their internal dynamics must always be considered when analyzing low temperature spectra.[30,32] In any case, the clear emergence of these crosspeaks – which are elusive under conventional high-field MAS NMR – at cryogenic conditions but slightly elevated temperature demonstrates the power of DNP signal enhancement even at the relatively low field of 9.4 T to detect such contacts over relatively long distances if appropriate isotope labeling strategies are employed.

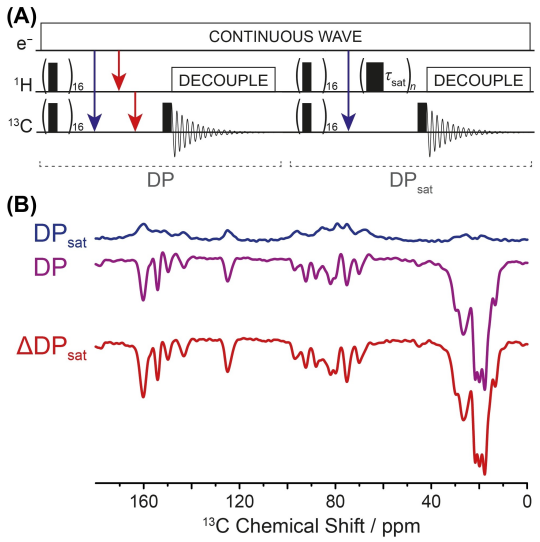

Figure 4. A) SCREAM-DNP pulse sequence using interleaved acquisition of DP and DP_{sat} spectra. Each block is preceded by a saturation train of 16 90° pulses that delete any residual magnetization before the polarization period during which, exclusively in the DP_{sat} block, 180° inversion pulses with an interpulse delay, τ_{sat}, of 250 ms are effectively quenching heteronuclear cross-relaxation transfer (red arrows). This allows efficient mathematical subtraction of magnetization on ^{13}C from direct DNP (blue arrows). B) Example DP, DP_{sat}, and the resulting ΔDP_{sat} spectra of the δ-$^{13}CH_3$ ILV-L7Ae-wt + ^{2}H,^{13}C,^{15}N A^{lab}, ^{2}H U,G,C^{lab} RNA complex at 145 K after 8 s of polarization time.

In Figure 4 we show the pulse sequence (panel A) used to record a spectrum which contains exclusively polarization generated by the spontaneous transfer of the enhanced polarization of methyl ^{1}H to ^{13}C by SCREAM-DNP (panel B). This is achieved by recording the direct polarization (DP) of ^{13}C using a Bloch decay (single pulse excitation) after a sufficiently long buildup period of in this case 8 s, during which ^{1}H DNP as well as the subsequent ^{1}H,^{13}C cross-relaxation transfer occurs. In order to suppress competing direct DNP of ^{13}C which cannot be removed by phase cycling, an equivalent spectrum is recorded under identical conditions but with saturation of ^{1}H spins during the buildup period (DP_{sat}). Mathematical subtraction of these two spectra then yields the pure contribution from SCREAM-DNP (ΔDP_{sat}). Here, interleaved acquisition of the two experiments prevents artifacts due to drift of sample temperature and/or probe tuning between these experiments, particularly if their difference due to SCREAM-DNP may be small compared to the direct DNP contribution. In our case, we have found rather large signal enhancement by SCREAM-DNP at the elevated temperatures accessed experimentally and only very small direct DNP signal; nevertheless, for quantitative analysis subtraction of the latter was still necessary.

In Figure 5A we show only the mathematically isolated SCREAM-DNP signals (ΔDP_{sat}) for different buildup periods between 0.5 and 512 s. Note, that the methyl signals appear significantly faster than all other signals, with almost complete buildup of intensity after just a few seconds whereas the adenosines' spectral contributions consisting of the ribose area

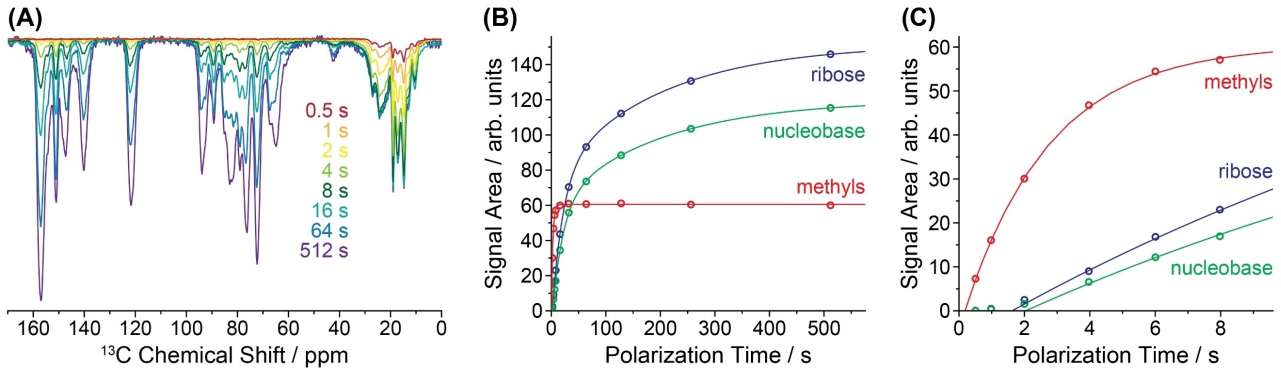

Figure 5. A) SCREAM-DNP spectra of the δ-$^{13}CH_3$ ILV-L7Ae-wt + ^{2}H,^{13}C,^{15}N A^{lab}, ^{2}H U,G,C^{lab} RNA complex at different polarization times. B) Buildup curves obtained by integration over the nucleobase, ribose, and methyl regions (Figure 2). C) Magnification of the early polarization buildup showing the immediate exponential buildup of methyl resonances but the delayed buildup of nucleotide resonances after a significant induction period. All fitting parameters are given in Table S2.

between 60 and 100 ppm and the nucleobase resonances between 120 and 165 ppm appear visibly later, after the methyls have significantly built up inverted polarization. Fitting of all integrated methyl peaks with a monoexponential buildup function have yielded a time constant of 2.6 s, whereas for the integral over the full nucleobase or ribose region a biexponential buildup function was required with fast and slow time constants of ~20 and ~200 s, respectively, with an area ratio close to unity (Table S2). For the adenosine resonances we have also observed a short average induction period of ~2 s before the exponential buildup starts; the methyls show no visible lag. The respective buildup curves in Figure 5B and C clearly depict this behavior. We interpret this as a telltale sign of the initial polarization transfer from methyl-^{1}H to methyl-^{13}C which is required before spin-diffusion may relay this polarization from the methyls to the nucleotide carbons. Furthermore, we attribute the short exponential time constant of the adenosine signals to the sought-after SCREAM-DNP transfer chain by cross-relaxation within ^{13}C-methyls and subsequent relay to the directly dipolar coupled adenosines. The origin of the second, slower components is less clear. Note, that by integrating over these large spectral regions we only observe an averaged buildup of all adenosines present in the RNA. Therefore, it may be due to one or more additional, less specific transfer pathways. First, unlabeled methyl-bearing amino acids (i.e., Ala, Thr, and Met) statistically carry ^{13}C in natural abundance; in this case, the overall transfer should follow the same mechanism and similar dynamics as we observe for ^{13}C-labeled ILV methyl (i.e., methyl-^{1}H to methyl-^{13}C by cross-relaxation and subsequent ^{13}C,^{13}C spin diffusion, albeit with a 90-fold reduction in intensity. Second, a much less efficient cross-relaxation transfer may also occur from any methyl group featuring ^{12}C, by direct dipolar contact between the methyl-^{1}H and any ^{13}C of adenosine.[20] A comparison of the SCREAM-DNP signal intensity of ^{13}C,^{15}N A^{lab} RNA in complex with δ-^{13}CH$_3$ ILV-L7Ae-wt and the complex containing na-L7Ae in natural isotope abundance (Figure S2) supports the hypothesis that a significant fraction of the slowly building up SCREAM-DNP signal is actually arising from the latter mechanism. Furthermore, slow, long-range spin diffusion between nucleotides within the deuterated RNA may also contribute to this component.

A comparison between a CPMAS spectrum and a ΔDP_{sat} spectrum emphasizes the specificity of the SCREAM-DNP mechanism. Whereas the CPMAS spectrum shows contributions from all 8 adenosines in the 26mer RNA and consequentially large inhomogeneous broadening, the ΔDP_{sat} spectrum is much better resolved due to a smaller number of contributing nucleotides. Notably, we observe strong deviations in the ribose regions with respect to the peak maxima in the CP spectrum. These deviations are in agreement with different ribose puckers, either existing in the north (3′-*endo*) or the south (2′-*endo*) conformation.[33] In Figure 6A, we have marked the expected chemical shift ranges from canonical nucleotide conformation in the CP spectrum, which coincide well with the experimental peak maxima of the CP spectral envelope, indicating that the majority of riboses are in canonical conformation. In contrast, in the ΔDP_{sat} spectrum the peak positions suggest that a major

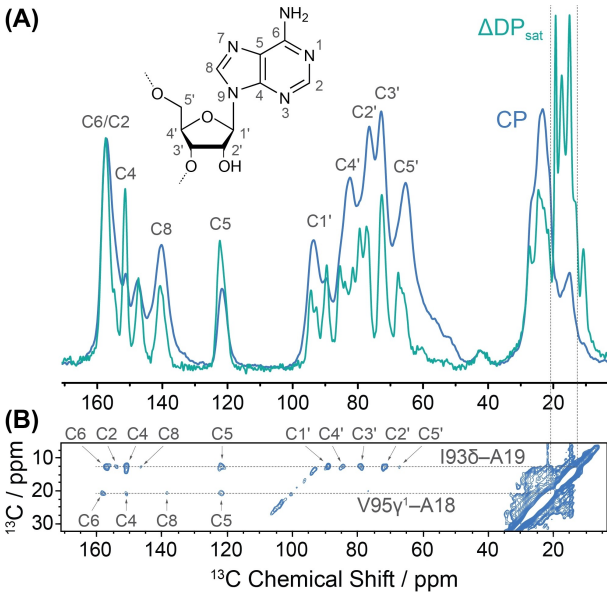

Figure 6. A) Comparison between the DNP-enhanced CPMAS spectrum (blue, see Figure 2) and the SCREAM-DNP spectrum (turquoise, see Figure 5) after 16 s of polarization time; the latter has been inverted for easier comparison. The peak maxima of the atoms within nucleotides in canonical conformation are marked above (see inset for atom numbering). B) This subregion from the DARR spectrum shown in Figure 3 shows clear congruence between the contacts emerging from I93δ methyl with well-resolved resonances in the SCREAM-DNP spectrum that deviate from the crowded and unresolved peak envelope in the CPMAS spectrum.

contribution of the SCREAM-DNP transfer is obtained on at least one adenosine in the noncanonical (south) puckering conformation. Earlier works have shown that only two of the eight adenosines are structured in this pucker: A5 and A19 which form a base-stacking interaction near the protein-RNA binding site.[29a] In contrast, A15, A18, and A22 are in the canonical (north) pucker, while the loop containing A11–A13 is unstructured.

Comparison of the resonances selectively enhanced by SCREAM-DNP with the crosspeak positions in the 2D DARR spectrum recorded after CP transfer (Figure 6B) shows a significant congruence of several predominant peaks of the ΔDP_{sat} spectrum with contacts to methyl group I93δ. Here, most striking is the unique shift of C1′ (89 ppm) which is very strongly upfield shifted with respect to its typical canonical chemical shift (93.5 ppm). Based on the assignments of a previous study,[29a] this peak which appears prominently in the DARR and also the ΔDP_{sat} spectrum is unambiguously attributed to A19. Furthermore, all observed contacts to I93δ in the DARR spectrum show excellent agreement with the assigned chemical shifts for A19, most notably the strongly downfield-shifted C8 (146.1 ppm) and C4′ (84.6 ppm). Note, that the latter resonance also appears as a unique resonance in the ΔDP_{sat} spectrum. C5′ is only showing a weak crosspeak in the DARR correlation spectrum, however, a prominent peak at 67.6 ppm in the ΔDP_{sat} spectrum coincides perfectly with the reported shift of 67.4 ppm for A19–C5′ and is substantially deshielded with respect to the CP envelope maximum occurring at the

expected canonical shift of ~65 ppm. This shows that I93δ is exclusively in dipolar contact with carbons from A19 and magnetization is preferentially transferred to A19 in a SCREAM-DNP experiment due to the close contact between the methyl and several carbon atoms of the nucleotide as depicted in Figure 7A.

By analysis of the SCREAM-DNP buildup behavior we may extract additional information supporting the above-discussed specificity of the transfer and the serially relayed transfer dynamics. In Figure 7B, we show a comparison of 5 different ΔDP_{sat} spectra recorded after 4, 8, 16, 64, and 512 s of polarization buildup. These spectra have been normalized to the intensity of the adenine–C6 resonance. This normalization allows us to differentiate three different sets of resonances according to their relative buildup behavior: i) those that build up in a similar manner to C6, ii) those that build up considerably faster than C6 and then level off quicker at longer polarization times, and iii) those that take considerably longer to polarize than C6. The condition (i) applies for all resonances which show similar intensities over all polarization times (marked by a gray "equal" sign). Resonances belonging to the group (ii) are easily identified by showing a reduction of the relative intensity with increasing polarization periods; several clear examples are marked by green downward pointing arrows. Finally, resonances which show a considerable increase in relative intensity belong to the group (iii) and are marked by a red upward arrow. Below the spectra we have also included a stick representation of the full set of expected resonance positions based on our previous work.[29a] Note that these assignments only include the nucleotides in the structured part of the 26mer RNA (i.e., A5, A15, A18, A19, and A22) and exclude nucleotides in the unstructured loop (i.e., A11–A13).

In group (i) we find the respective ribose carbon in the endo position (i.e., C3′ for north or C2′ for south puckers) at ~72 ppm, C5, and (obviously) C6. For all those resonances we see rather small chemical shift dispersion for all assigned nucleotides or in different words, we observe the average buildup behavior for all contributing nucleotides. For group (ii), we find, most prominently, the unique resonances of A19, including C1′, C4′, and C5′, where no significant overlap with other nucleotides is expected. Additionally, another resonance is found in agreement with the position of C3′ of A19 which overlaps with the expected chemical shifts of C2′ (and to some extent C3′) of A5. However, we find no indication for a

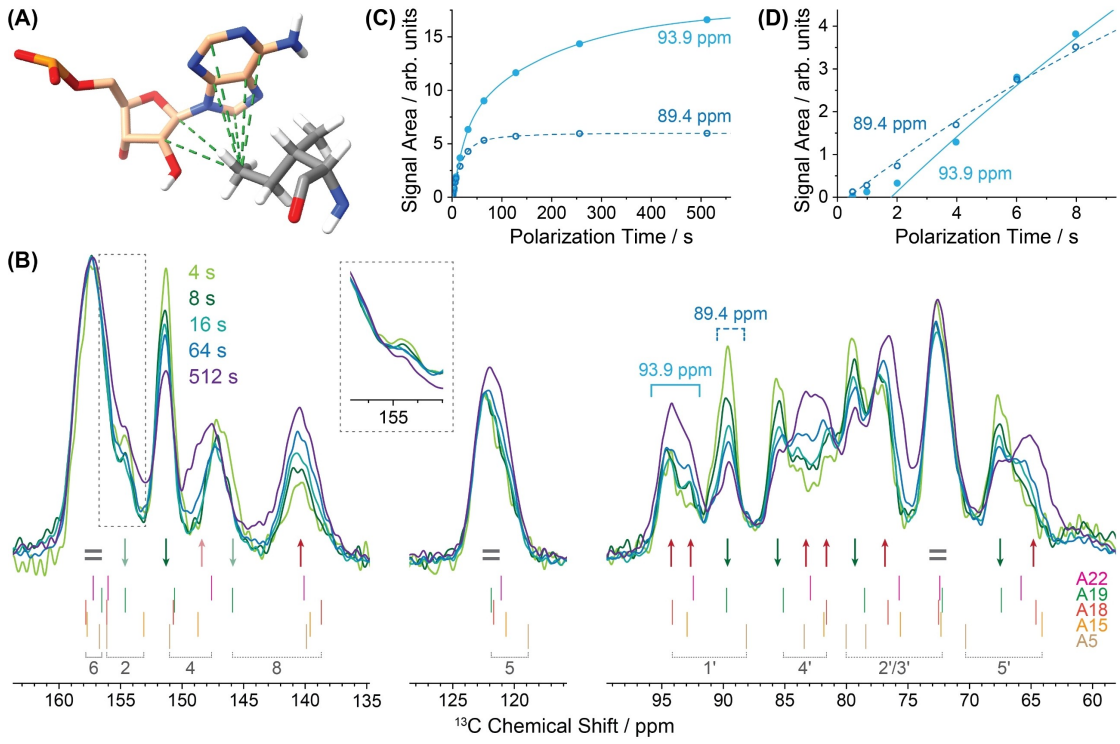

Figure 7. A) Depiction of the contact between I93 (gray carbon atoms) and A19 (light brown carbon atoms) based on model 2 out of a bundle of ten of the PDB structure 6TPH.[29b] Contacts between I93δ and adenosine carbons with an average distance shorter than 5 Å are shown by green dashed bonds. Color code of heteroatoms: red, oxygen; blue, nitrogen; orange, phosphorous; white, hydrogen. B) SCREAM-DNP spectra of the δ-$^{13}CH_3$ ILV-L7Ae-wt + $^{2}H,^{13}C,^{15}N$ A^{lab}, ^{2}H U,G,C^{lab} RNA complex at different polarization times normalized to the peak amplitude of C6. Spectra were taken from Figure 5; and inverted for better visibility. Spectral regions with a faster buildup than the C6 envelope are marked by green downward arrows, those with a slower buildup by red upwards arrows. Light arrows mark regions with the same tendency but severe overlap with other peaks. Gray equal signs mark peaks with similar buildup dynamics to the C6 envelope. Colored sticks below the spectra mark the assigned resonances for A5, A15, A18, A19, and A22 reported earlier.[29b] The dashed box marks the spectral regions shown in the insert, where the spectra have been scaled such that their shoulders match to show the relative decrease of the unique A19–C2 resonance at longer polarization times. C) Example buildup curve for the spectral regions marked in (B); D) Magnification of the early buildup curves showing the significantly reduced induction period for A19–C1′. The full set of buildup curves is shown in Figure S3, and the fitting parameters are given in Table S2.

significant contribution of other unique A5 ribose resonances (e.g., C1′ or C5′), leading us to believe that A5 does not significantly contribute to the spectrum at all. In the nucleobase region, assignments are generally overlapping more, but some clear observations can still be made: C4 shows a very fast buildup even though all nucleotides overlap at this resonance position. We attribute this to the very short I93δ–A19–C4 distance of only 3.9 Å which seems to dominate the buildup of all other contributing nucleotides. More quantitative analysis of the buildup dynamics shows that the integral area over their narrow, selective chemical shift ranges follows an almost monoexponential trend with a buildup time constant of ~20 s while the slow component of ~200 s was strongly attenuated with respect to the average behavior, as can be seen in the SI. Most notably, the induction period was also strongly reduced, leading to an almost instantaneous buildup and absolutely larger signal intensity compared to the spectral regions not containing contributions from A19. Further indications for relatively fast buildup are found for A19–C2 which is visible inside the shoulder of the much larger C2/C6 resonance (see insert in Figure 7) and A19–C8 with a rather unique chemical shift (145.8 ppm), however, this latter contribution seems only to be visible as an apparent upfield shift of the overlapping peak with A15–C4 and A22–C4 (~148 ppm) at shorter polarization times. Due to the ambiguous nature of these overlapping peaks we have marked these relative deviations with light arrows. For the last group (iii), we find strong deviations towards slower buildup at ribose resonance positions of A15/A18–C5′, A18–C2′, all C4′ resonances except that from A19, and, most strikingly, a strong contribution from all C1′ resonances except A19 and A5. For the adenosine resonances, we see such behavior for all C8 which overlap at ~140 ppm with the exception of A19, and the (already discussed) less clear deviation in the A15/A22–C4 buildup.

From these observations we can draw the following conclusions: a) A19 is clearly the dominating contributor at shortest buildup times, confirming that the fastest, initial SCREAM-DNP transfer originates from I93δ and is from there selectively transferred to A19. b) The overall envelope at intermediate times shows significant contributions from A18 which we expect to also being subject to efficient SCREAM-DNP transfer from V95γ1, however, due to the alternating labeling scheme of the two valine methyl groups, this is (at best) limited to 50% of all nucleotides in the sample. Nevertheless, a reduction in labeling efficiency should only reduce the magnitude of the transferred polarization and not the dynamics. As unique resonances of A18 show a relatively slower buildup than those of A19, this seems to indicate that in fact the SCREAM-DNP efficiency of the V95γ1–A18 transfer is less efficient than that of I93δ–A19. Since we would expect to find a significantly more efficient dipolar transfer from the V95γ1 methyl to the nucleobase of A18 based on the expected internuclear distances we believe that this is caused by the methyl dynamics of V95γ1 being less supportive for cross-relaxation as compared to I93δ. This interpretation is in agreement with our earlier observation that the primary (δ) methyl group of isoleucine is dynamically more active and builds up polarization through SCREAM-DNP significantly faster than both of the valine methyls.[20] c) Finally, we find no indication of a significant SCREAM-DNP contribution of A5 which should be identifiable due to several unique expected resonance positions of this nucleotide. This is surprising because this nucleotide is in direct base stacking interaction with A19 and, therefore, we would expect to see some relayed transfer through spin diffusion, particularly after the long polarization buildup period of 512 s. The reason for this, besides the non-negligible contribution from unspecific spectral contributions is unclear.

As the resonances of A19–C1′, –C4′, and –C5′ allow for individual integration over their peaks with only minor contributions from other resonances, we were able to analyze their buildup dynamics quantitatively. For a full representation of all buildup curves see Figure S3, and the fitting parameters in Table S2. The buildup curve for A19–C1′ is also exemplarily shown in Figure 7C, in comparison with the integrated region over all other C1′ resonances. While the fast components' buildup time constants from the A19-specific resonances show only an insignificant reduction as compared to the respective non-specific spectral regions (18–21 vs. 18–24 s) we have found a diminished relative contribution of the slowly building up component by up to a factor of 5, while the slow buildup time constants were also effectively conserved within their now larger error margins. At the same time, the time lag before the exponential buildup is significantly reduced for the A19-specific resonances (see Figure 7D for C1′ as an example). Besides being clearly observable for the distinguished C1′, C4′, and C5′ resonances, this behavior is also found for the spectral region where the unique chemical shifts of C3′ and C4 are expected, however, with smaller significance due to the larger spectral overlap with other resonances. This overall behavior leads us to believe that the direct dipolar contact between I93δ and A19 caused a ^{13}C–^{13}C polarization exchange on the timescale of 20 s while unspecific scrambling of ^{13}C magnetization over the large ^{13}C network by spin diffusion gives rise to the slowly building up contribution on the timescale of 200 s.

Next, we could successfully extract further information about the spontaneous polarization transfer during SCREAM-DNP by variation of MAS frequency. By increasing the sample rotation rate, spin diffusion may be strongly suppressed by decoupling of homonuclear dipole-dipole interactions. As shown in Figure 8, at 14 kHz for δ-$^{13}CH_3$ ILV-L7Ae-wt + ^{2}H,^{13}C,^{15}N A^{lab}, ^{2}H U,G,C^{lab} RNA complex, the signal clearly builds up first on the adenine base before it becomes slowly visible on the ribose resonances. This confirms, that indeed under these conditions the methyl group transfers its polarization first to the nucleobase to which it is on average much closer than it is to the ribose ring. This also shows that the homonuclear transfer from the methyl can be furthermore controlled by frequency-selective recoupling using rotational resonance (R^2) as the MAS frequency of 14 kHz fulfills the R^2 condition between methyls and nucleobase resonances.[34] A publication on this topic is currently under preparation and will be published elsewhere.

Furthermore, comparison with the I93C mutant in which the major methyl polarization source for SCREAM-DNP has been

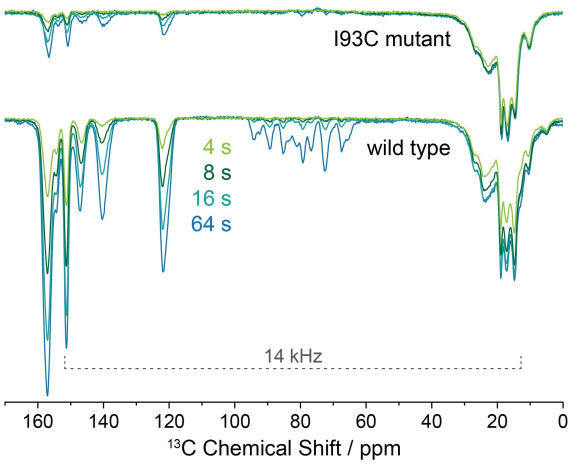

Figure 8. Comparison between SCREAM-DNP spectra of the δ-$^{13}CH_3$ ILV-L7Ae-wt and δ-$^{13}CH_3$ ILV-L7Ae-I93C, each in complex with ^{2}H,^{13}C,^{15}N A^{lab}, ^{2}H U,G,C^{lab} RNA recorded at 14 kHz MAS and at different polarization times. The R^2 condition with I93δ is marked by a gray bracket.

substituted by a cross-relaxation inactive –SH side chain shows a drastically reduced overall intensity on all nucleotide signals in a ΔDP_{sat} spectrum. The I93C mutation does not significantly alter the binding affinity (see isothermal titration calorimetry results in the SI) and has shown, by earlier PRE experiments,[29b] to preserve the protein–RNA interface. Therefore, the signal intensity reduction of ~80% furthermore proves that I93δ contributes for, by far, the largest amount of SCREAM-DNP polarization on the RNA whereas contributions from other methyls only add to not more than 20% (Figure 8), and even less if the above-mentioned boost in homonuclear transfer efficiency by R^2 is avoided (Figure S4). In light of the occurrence of only one further set of methyl–RNA contacts, namely V95γ1–A18, in the DARR spectrum in combination with the short methyl–adenine distances structurally modeled for this contact, we postulate that a significant fraction of these remaining SCREAM-DNP transfer pathways are induced by this methyl group, despite its non-ideal methyl dynamics.[20] However, a large number of small, nonspecific SCREAM-DNP transfer pathways from ILV-labeled methyls or methyls in natural abundance may still contribute to the observed spectrum.

Conclusions

We have shown that a single methyl group is responsible for a large majority of DNP-enhanced magnetization spontaneously transferred by heteronuclear cross-relaxation from ^{1}H of the protein to ^{13}C of the RNA across the binding interface in an RNP complex. The identification of such a dipolar contact over a distance of 4 Å and more by SCREAM-DNP is robust and can be performed in a short amount of time in a 1D spectral acquisition, as the resonances obtained in a ΔDP_{sat} spectrum emerge very specifically from such transfer pathways and virtually no spurious background signals hamper the detection even of small signals over a large potential background of SCREAM-DNP-inactive sites. Recording homonuclear correlation spectra by spin diffusion over these rather large distances suffers from longitudinal relaxation during the long mixing periods required, thus limiting its applicability.

Furthermore, an applied orthogonal protonation/deuteration scheme of protein and RNA was selected and proven, on the one hand, to maximize ^{1}H spin diffusion within the protein, while, on the other hand, to minimize ^{13}C magnetization scrambling by proton-driven spin diffusion within the RNA. This guarantees the efficient transport of enhanced polarization from the DNP polarizing agent to the dynamically active methyl groups so that the ^{1}H–^{13}C cross relaxation results in optimal ^{13}C SCREAM-DNP enhancement. Our results indicate that the protons of the methyl group efficiently drive spin diffusion to the directly coupled ^{13}C of the RNA; however, subsequent relayed spin diffusion, most particularly inter-residue transfer over medium to large distances, is attenuated. This motion-activated transfer mechanism thus leads to a large degree of local specificity of the accrued ^{13}C polarization. Furthermore, frequency-selective recoupling by R^2 principally allows the transfer to be directed, for example, to certain nucleotides based on matching their chemical shift difference with respect to the methyl group to the MAS frequency. This could be further used to select a specific transfer pathway over others. Such a highly localized generation of ^{13}C polarization over a large distance within the interaction site could then, for example, be combined with multidimensional correlation spectroscopy to selectively extract unique structural information from contact surfaces over shorter distances, without spectral crowding from unwanted parts of the biomolecular complex.

Additional potential in optimizing or selecting for specific pathways lies in the variation of experimental parameters such as temperature or polarization buildup time. In this study, we have already shown that transfers over short distances can be preferentially enhanced by choosing short polarization periods that also allow faster recycling and accumulation of transients. By optimizing this parameter, a maximum specificity for the shortest distance(s) might be achieved. Furthermore, controlling the sample temperature could be an important tool in selecting only specific methyl groups by bringing their dynamics into a more supportive regime for cross relaxation than others. Here, we have shown that the more efficient SCREAM-DNP transfer by I93δ in comparison to V95γ1 correlates with the general buildup dynamics observed for the respective amino acids in frozen solution. However, this was done without careful optimization of sample temperature for maximum specificity, but for maximum methyl signal intensity in the CP spectra. Therefore, optimization of the sample temperature for maximum specificity could lead to further gains in this direction.

In conclusion, this study demonstrates that SCREAM-DNP is able to provide highly selective transfer of polarization over intermediate distances between biomolecular subunits in RNPs without the need for site-specific isotope labeling. We have shown that well-established biochemical sparse isotope labeling schemes such as ILV-methyl labeling for the protein- or nucleotide-type-specific labeling of RNA by in vitro transcription

can yield suitable conditions such that a single methyl–nucleotide contact dominates the SCREAM-DNP transfer. Thus, no a priori knowledge of the binding site structure is necessary to deduce a labeling scheme. Hypothesis-based experiments could then be performed on a single sample (i.e., with only one labeled nucleotide type), or a more general probing of contacts could be performed by permutating the type of ^{13}C-labeled nucleotide, requiring a maximum of four RNA samples to be synthesized by in vitro transcription.

Experimental Section

L7Ae-RNA complex preparation

Materials: All the reagent grade chemicals used in this study were acquired either from Carl Roth or Sigma-Aldrich. The stable isotope-labeled precursor compounds for $^{13}CH_3$-ILV-labeling were obtained from Sigma-Aldrich. Uniform ^{2}H-labeled, ^{13}C,^{15}N-labeled and ^{2}H-,^{13}C-,^{15}N-labeled rNTPs were obtained from Silantes. See the Supporting Information for further information.

Wild type and I93C L7Ae expression: L7Ae construct was prepared as described elsewhere.[27] I93C L7Ae mutant was selected based on the structure of L7Ae-Box C/D RNA complex (PDB ID 6TPH).[29b] The protein was prepared by recombinant overexpression from *Escherichia coli*. For the expression of unlabeled protein (na-L7Ae), a preculture was added to LB medium and grown at 37 °C before induction by isopropyl-β-D-1-thiogalactopyranoside (IPTG) and further growth at 20 °C. For the preparation of δ-$^{13}CH_3$ ILV-L7Ae, the preculture was resuspended in H_2O-based minimal medium. The culture was grown at 37 °C and, before induction, labeled isotopic precursors were added as 60 and 120 mg L^{-1} of 2-ketobutyric acid-4-^{13}C-3,3-d_2 sodium salt hydrate and 2-keto-3-(methyl-d_3)butyric acid-4-^{13}C,3-d sodium salt, respectively, at 20 °C. Induction of the cells was obtained with 1 mM IPTG and continued to grow at 20 °C. In both cases the cells were finally harvested by centrifugation and the pellet was resuspended in 1×PBS and frozen at −20 °C until further use. L7Ae was purified using denaturation and refolding purification protocol that was optimized in our laboratory.[29b] See the Supporting Information for detailed preparation and purification protocols.

Box C/D 26mer RNA synthesis: For all measurements, nucleotide-type selective Box C/D 26mer RNA (5′-GCUGAGCUCGAAAGA-GCAAUGAUGUC-3′) was prepared by in vitro transcription using in-house produced T7 RNA polymerase, NTPs and synthetic DNA oligos or plasmid DNA. Nucleotide-type-specific labelled RNA were obtained using rNTP mixtures of unlabeled, ^{2}H- or ^{13}C,^{15}N-labeled or ^{2}H,^{13}C,^{15}N labeled rNTPs. The optimized conditions were selected and typically 5–10 mL large reactions were performed.[35] The RNA was purified by denaturing polyacrylamide gel electrophoresis and extracted from the gel by crash and soak method or electroelution.[36] The pure RNA was then dissolved in water, tested for RNAse contamination and stored at −20 °C. Finally, two different labeled RNA were prepared: ^{13}C, ^{15}N A^{lab} RNA and ^{2}H,^{13}C,^{15}N A^{lab} + ^{2}H U,G,C^{lab} RNA. See the Supporting Information for detailed preparation and purification protocols.

L7Ae–RNA complex formation: The L7Ae–RNA complex was prepared by mixing the L7Ae protein and the 26mer RNA at a molar ratio of 1:1.1. The mixture was incubated at 80 °C for 15 min, followed by cool-down to room temperature and centrifugation to remove possible high molecular agglomerates. The L7Ae–RNA complex was separated from dimers and excess of unbound RNA by size-exclusion chromatography (SEC). SEC fractions corresponding to monomeric complex were concentrated and stored at 4 °C until used. Samples prepared for DNP experiments were: a) na-L7Ae-wt + ^{13}C,^{15}N A^{lab} RNA complex; b) δ-$^{13}CH_3$ ILV-L7Ae-wt + ^{13}C,^{15}N A^{lab} RNA complex; c) δ-$^{13}CH_3$ ILV-L7Ae-wt + ^{2}H,^{13}C,^{15}N A^{lab}, ^{2}H U,G,C^{lab} RNA complex; d) δ-$^{13}CH_3$ ILV-L7Ae-I93C + ^{2}H,^{13}C,^{15}N A^{lab}, ^{2}H U,G,C^{lab} RNA complex. See the Supporting Information for a detailed protocol.

Isothermal titration calorimetry: ITC experiments were carried out on a Nano ITC machine (TA Instruments) in 25 mM HEPES (pH 7.5), 120 mM NaCl, 1 mM TCEP at 30 °C. K_D values were calculated from a single replicate using a single binding site model, yielding 4.4 nM for L7Ae-wt and 5.3 nM for L7Ae-I93C mutant, respectively. For further experimental details and a full results table as well as titration curves, see the Supporting Information.

Sample preparation for DNP experiments: L7Ae–RNA complexes were lyophilized and then reconstituted in d_8-$^{12}C_3$-glycerol (98 % ^{2}H, 99.95 % ^{12}C, Euriso-Top)/D_2O/H_2O (50:40:10 vol.–%) mixture containing 15 mM, if not mentioned otherwise, dissolved AMUPol[37] (SATT Sud-Est, Marseille) so that the final solution resulted in a complex concentration of ~0.4 mM for samples a), b) and c), and ~0.2 mM for the sample d). Samples were then transferred into a 1.3 or a 3.2 mm sapphire MAS sample rotor (Bruker) closed with a vespel drive cap.

NMR spectroscopy

Conventional ^{13}C ssNMR spectroscopy: Two-dimensional ^{13}C,^{13}C RFDR NMR experiments were performed on a 600 MHz Bruker AVANCE III HD spectrometer using a commercial 3.2 mm ^{1}H/^{13}C/^{15}N MAS probe at an MAS rate of 14 kHz. Adjacent carbons were correlated using RFDR mixing scheme of 14 ms length with XY-8 phase cycle.[38] High-power proton decoupling during RFDR mixing was performed using the frequency-switched Lee-Goldburg (FSLG) sequence,[39] while SPINAL-64 decoupling at 89 kHz was used during ^{13}C evolution and detection. 256 scans were accumulated per t_1 slice at a recycle delay of 3 s. For further information including rf pulse strengths, as well as evolution, acquisition and postprocessing parameters, see the Supporting Information.

DNP-enhanced MAS NMR spectroscopy: DNP experiments for data shown in Figures 2–4, S1 and S2 were performed using a commercially available Bruker AVANCE II DNP spectrometer operating at 400.2 MHz ^{1}H frequency with a Bruker Ultrashield 9.4 T wide bore (89 mm) magnet and 263.4 GHz microwave frequency produced by a Bruker fundamental-mode gyrotron with 60 mA of beam current. The temperature was read out from a thermocouple inside the MAS stator. SPINAL-64 at 100 kHz was used for broadband decoupling of ^{1}H. MAS with a spinning frequency of 8 kHz was used for all experiments, if not mentioned otherwise. The used pulse sequences for SCREAM-DNP experiments were analogous as described elsewhere.[20,24]

The DARR experiments were performed at 8 kHz MAS. 32 scans were accumulated per t_1 slice at a recycle delay of 4 s. DARR recoupling power was set to the $\omega_{1,H} = \omega_r$ condition, with $\omega_{1,H}$ being the ^{1}H Rabi frequency.

SCREAM-DNP experiments shown in Figures 4, 6, 7, S3, and S4 were performed on a Bruker AVANCE III HD spectrometer operating at 400.2 MHz proton frequency with a Bruker ASCEND DNP 9.4 T wide-bore (89 mm) magnet and 263.4 GHz microwave frequency produced by a Bruker second-harmonic gyrotron with 132 or 138 mA of beam current. SPINAL-64 ^{1}H decoupling was used during acquisition. The used pulse sequences for SCREAM-DNP experiments were analogous as described elsewhere.[20,24] For acquiring the DP_{sat} spectrum, an additional 180° ^{1}H pulse was applied every

250 ms to prevent ^{1}H polarization buildup during the ^{13}C polarization time. The MAS frequency was set to 14 kHz and the four experiments per sample (4, 8, 16, and 64 s polarization time) were conducted at a sample temperature of 140 K as given by the probe's internal temperature sensor inside the stator.

For further information on all experiments, including rf pulse strengths, as well as evolution, acquisition and postprocessing parameters, see the Supporting Information.

SCREAM-DNP data analysis: ΔDPsat spectra were obtained by mathematical subtraction in Bruker Topspin 4.0.7. Spectral regions were then integrated with OriginPro 2022b, and the integrals were fitted with bi-exponential functions according to Equation (S1). For the methyl region, a mono-exponential function was used as given in Equation (S2). In order to account for delays in polarization buildup resulting from induction periods due to the serial transfer of polarization, first building up on ^{1}H, then propagating from methyl-^{1}H to ^{13}C, and finally exchanging between ^{13}C, we have introduced a time offset. No ordinate offset was necessary for obtaining satisfactory fits with coefficients of determination (R^2) of at least 0.999 (Table S2). For detailed spectral processing protocols and fitting equations, see the Supporting Information.

Acknowledgments

This work was funded by the Deutsche Forschungsgemeinschaft (DFG) through research grants CO 802/4-1 and MA 5157/3-1 and through large instrument grant INST 264/177-1 FUGG. Further support was provided by the German Federal State of Hesse through the Center for Biomolecular Magnetic Resonance (BMRZ), Frankfurt am Main. We thank Johanna Becker-Baldus and Clemens Glaubitz (Frankfurt) for support and access to the MAS DNP instrument. TB acknowledges support by the Joachim Herz Foundation through an Add-on Fellowship for Interdisciplinary Life Sciences. Open Access funding enabled and organized by Projekt DEAL.

Conflict of Interest

The authors declare no conflict of interest.

Data Availability Statement

The data that support the findings of this study are available from the corresponding author upon reasonable request.

Keywords: dynamic nuclear polarization · isotopic labeling · NMR spectroscopy · proteins · RNA

[1] E. Lionta, G. Spyrou, K. D. Vassilatis, Z. Cournia, *Curr. Top. Med. Chem.* **2014**, *14*, 1923–1938.
[2] a) S. Ahlawat, K. R. Mote, N.-A. Lakomek, V. Agarwal, *Chem. Rev.* **2022**, *122*, 9643–9737; b) A. McDermott, *Annu. Rev. Biophys.* **2009**, *38*, 385–403; c) S. K. Vasa, P. Rovó, R. Linser, *Acc. Chem. Res.* **2018**, *51*, 1386–1395.
[3] a) A. Schuetz, C. Wasmer, B. Habenstein, R. Verel, J. Greenwald, R. Riek, A. Bockmann, B. H. Meier, *ChemBioChem* **2010**, *11*, 1543–1551; b) M. T. Colvin, R. Silvers, B. Frohm, Y. Su, S. Linse, R. G. Griffin, *J. Am. Chem. Soc.* **2015**, *137*, 7509–7518.
[4] a) A. W. Overhauser, *Phys. Rev.* **1953**, *92*, 411–415; b) T. R. Carver, C. P. Slichter, *Phys. Rev.* **1953**, *92*, 212–213; c) B. Corzilius, *Annu. Rev. Phys. Chem.* **2020**, *71*, 143–170.
[5] a) A. S. Lilly Thankamony, J. J. Wittmann, M. Kaushik, B. Corzilius, *Prog. Nucl. Magn. Reson. Spectrosc.* **2017**, *102–103*, 120–195; b) T. Biedenbänder, V. Aladin, S. Saeidpour, B. Corzilius, *Chem. Rev.* **2022**, *122*, 9738–9794; c) W. Y. Chow, G. De Paëpe, S. Hediger, *Chem. Rev.* **2022**, *122*, 9795–9847.
[6] K. Pervushin, R. Riek, G. Wider, K. Wüthrich, *Proc. Natl. Acad. Sci. USA* **1997**, *94*, 12366–12371.
[7] a) V. Tugarinov, P. M. Hwang, J. E. Ollerenshaw, L. E. Kay, *J. Am. Chem. Soc.* **2003**, *125*, 10420–10428; b) V. Tugarinov, P. M. Hwang, L. E. Kay, *Annu. Rev. Biochem.* **2004**, *73*, 107–146.
[8] a) R. Sprangers, L. E. Kay, *Nature* **2007**, *445*, 618–622; b) G. Mas, J.-Y. Guan, E. Crublet, E. C. Debled, C. Moriscot, P. Gans, G. Schoehn, P. Macek, P. Schanda, J. Boisbouvier, *Sci. Adv.* **2018**, *4*, eaau4196.
[9] V. Tugarinov, L. E. Kay, *J. Am. Chem. Soc.* **2003**, *125*, 13868–13878.
[10] D. Neuhaus, M. P. Williamson, *The Nuclear Overhauser Effect in Structural and Conformational Analysis*, 2nd ed., Wiley-VCH, Weinheim, **2000**.
[11] I. Solomon, *Phys. Rev.* **1955**, *99*, 559–565.
[12] a) M. G. Gibby, A. Pines, J. S. Waugh, *Chem. Phys. Lett.* **1972**, *16*, 296–299; b) A. Naito, C. A. McDowell, *J. Chem. Phys.* **1986**, *84*, 4181–4186; c) J. L. White, J. F. Haw, *J. Am. Chem. Soc.* **1990**, *112*, 5896–5898.
[13] a) N. Giraud, J. Sein, G. Pintacuda, A. Böckmann, A. Lesage, M. Blackledge, L. Emsley, *J. Am. Chem. Soc.* **2006**, *128*, 12398–12399; b) J. M. Lopez del Amo, V. Agarwal, R. Sarkar, J. Porter, S. Asami, M. Rübbelke, U. Fink, Y. Xue, O. F. Lange, B. Reif, *J. Biomol. NMR* **2014**, *59*, 241–249.
[14] a) J. L. White, *Solid State Nucl. Magn. Reson.* **1997**, *10*, 79–88; b) R. Zhang, Y. Nishiyama, A. Ramamoorthy, *J. Magn. Reson.* **2019**, *309*, 106615.
[15] A. Lesage, L. Emsley, F. Penin, A. Böckmann, *J. Am. Chem. Soc.* **2006**, *128*, 8246–8255.
[16] a) K. Takegoshi, T. Terao, *J. Chem. Phys.* **2002**, *117*, 1700–1707; b) S. E. Ashbrook, N. G. Dowell, I. Prokes, S. Wimperis, *J. Am. Chem. Soc.* **2006**, *128*, 6782–6783.
[17] a) E. Katoh, K. Takegoshi, T. Terao, *J. Am. Chem. Soc.* **2004**, *126*, 3653–3657; b) R. N. Purusottam, G. Bodenhausen, P. Tekely, *J. Biomol. NMR* **2013**, *57*, 11–19.
[18] a) D. Daube, V. Aladin, J. Heiliger, J. J. Wittmann, D. Barthelmes, C. Bengs, H. Schwalbe, B. Corzilius, *J. Am. Chem. Soc.* **2016**, *138*, 16572–16575; b) M. M. Hoffmann, S. Bothe, T. Gutmann, F.-F. Hartmann, M. Reggelin, G. Buntkowsky, *J. Phys. Chem. C* **2017**, *121*, 2418–2427.
[19] V. Aladin, B. Corzilius, *eMagRes* **2020**, *9*, 239–250.
[20] V. Aladin, B. Corzilius, *Solid State Nucl. Magn. Reson.* **2019**, *99*, 27–35.
[21] M. M. Hoffmann, S. Bothe, T. Gutmann, G. Buntkowsky, *J. Phys. Chem. C* **2017**, *121*, 22948–22957.
[22] H. Park, B. Uluca-Yazgi, S. Heumann, R. Schlogl, J. Granwehr, H. Heise, P. P. M. Schleker, *J. Magn. Reson.* **2020**, *312*, 106688.
[23] a) I. V. Sergeyev, C. M. Quinn, J. Struppe, A. M. Gronenborn, T. Polenova, *Magn. Reson.* **2021**, *2*, 239–249; b) P. Berruyer, M. Gericke, P. Moutzouri, D. Jakobi, M. Bardet, L. Karlson, S. Schantz, T. Heinze, L. Emsley, *Carbohydr. Polym.* **2021**, *262*, 117944.
[24] V. Aladin, M. Vogel, R. Binder, I. Burghardt, B. Suess, B. Corzilius, *Angew. Chem. Int. Ed.* **2019**, *58*, 4863–4868; *Angew. Chem.* **2019**, *131*, 4917–4922.
[25] J. Mao, V. Aladin, X. Jin, A. J. Leeder, L. J. Brown, R. C. D. Brown, X. He, B. Corzilius, C. Glaubitz, *J. Am. Chem. Soc.* **2019**, *141*, 19888–19901.
[26] W. A. Decatur, M. J. Fournier, *Trends Biochem. Sci.* **2002**, *27*, 344–351.
[27] A. Lapinaite, B. Simon, L. Skjaerven, M. Rakwalska-Bange, F. Gabel, T. Carlomagno, *Nature* **2013**, *502*, 519.
[28] J. F. Kuhn, E. J. Tran, E. S. Maxwell, *Nucleic Acids Res.* **2002**, *30*, 931–941.
[29] a) A. Marchanka, B. Simon, G. Althoff-Ospelt, T. Carlomagno, *Nat. Commun.* **2015**, *6*, 7024; b) M. Ahmed, A. Marchanka, T. Carlomagno, *Angew. Chem. Int. Ed.* **2020**, *59*, 6866–6873; *Angew. Chem.* **2020**, *132*, 6933–6940.
[30] a) Q. Z. Ni, E. Markhasin, T. V. Can, B. Corzilius, K. O. Tan, A. B. Barnes, E. Daviso, Y. Su, J. Herzfeld, R. G. Griffin, *J. Phys. Chem. B* **2017**, *121*, 4997–5006; b) A. H. Linden, W. T. Franks, U. Akbey, S. Lange, B. J. van Rossum, H. Oschkinat, *J. Biomol. NMR* **2011**, *51*, 283–292.
[31] C. Farès, I. Amata, T. Carlomagno, *J. Am. Chem. Soc.* **2007**, *129*, 15814–15823.
[32] Ü. Akbey, A. H. Linden, H. Oschkinat, *Appl. Magn. Reson.* **2012**, *43*, 81–90.
[33] a) M. Ebrahimi, P. Rossi, C. Rogers, G. S. Harbison, *J. Magn. Reson.* **2001**, *150*, 1–9; b) B. Fürtig, C. Richter, J. Wöhnert, H. Schwalbe, *ChemBioChem*

2003, *4*, 936–962; c) A. V. Cherepanov, C. Glaubitz, H. Schwalbe, *Angew. Chem. Int. Ed.* **2010**, *49*, 4747–4750; *Angew. Chem.* **2010**, *122*, 4855–4859.
[34] a) E. R. Andrew, S. Clough, L. F. Farnell, T. D. Gledhill, I. Roberts, *Physics Letters* **1966**, *21*, 505–506; b) D. P. Raleigh, M. H. Levitt, R. G. Griffin, *Chem. Phys. Lett.* **1988**, *146*, 71–76.
[35] J. F. Milligan, D. R. Groebe, G. W. Witherell, O. C. Uhlenbeck, *Nucleic Acids Res.* **1987**, *15*, 8783–8798.
[36] A. Marchanka, C. Kreutz, T. Carlomagno, *J. Biomol. NMR* **2018**, *71*, 151–164.
[37] C. Sauvée, M. Rosay, G. Casano, F. Aussenac, R. T. Weber, O. Ouari, P. Tordo, *Angew. Chem. Int. Ed.* **2013**, *52*, 10858–10861; *Angew. Chem.* **2013**, *125*, 11058–11061.
[38] Y. Ishii, *J. Chem. Phys.* **2001**, *114*, 8473–8483.
[39] A. Bielecki, A. C. Kolbert, H. J. M. De Groot, R. G. Griffin, M. H. Levitt in *Advances in Magnetic and Optical Resonance, Vol. 14* (Ed.: W. S. Warren), Academic Press, San Diego, **1990**, pp. 111–124.

Manuscript received: November 6, 2022
Accepted manuscript online: December 19, 2022
Version of record online: February 7, 2023